

Velocity-Dependent Dynamic Manipulability

Michael T. Rosenstein and Roderic A. Grupen

Department of Computer Science

University of Massachusetts

Amherst, MA 01003 USA

mtr@cs.umass.edu, grupen@cs.umass.edu

Abstract—Measures of dynamic manipulability summarize a manipulator’s capacity to generate accelerations for arbitrary tasks, and such measures are useful tools for the design and control of general-purpose robots. Existing measures, however, downplay the effects of velocity or else ignore them altogether. In this paper we derive the relationship between joint velocity and end-effector acceleration, and through case studies we demonstrate that velocity has a complex, non-negligible effect on manipulability. We also provide evidence that movement near a singularity is beneficial for certain tasks.

I. INTRODUCTION

Any suitable measure that summarizes the capabilities of a manipulator may provide useful information for both the design of multi-purpose robots and for the subsequent planning of efficient movements. Yoshikawa [1] suggested one such measure based on the volume of the *manipulability ellipsoid*, as derived from a manipulator’s kinematic properties, i.e., the Jacobian. Similarly, Chiu [2] viewed a manipulator as a “mechanical transformer” and used the Jacobian to describe the duality between velocity and force transmission capabilities. Chiu also defined the *compatibility index* as a basis for computing postures that optimize a robot’s performance at a particular task [2].

A number of extensions to this work dealt with dynamic, as well as kinematic characteristics of the robot. To quantify acceleration capabilities, for example, Yoshikawa later proposed the *dynamic manipulability measure* [3] which incorporates the manipulator mass matrix in addition to the Jacobian. Subsequently, Chiacchio and colleagues demonstrated that gravity induces a translation of the *dynamic manipulability ellipsoid* [4] and that a weighted Jacobian—one that accounts for inertia and torque limits—provides a better match between such ellipsoids and the corresponding acceleration polytopes [5].

Despite considerable progress with regard to measures of dynamic manipulability, relatively little attention has been paid to the effects of velocity-dependent dynamics, i.e., Coriolis and centrifugal forces. One exception is the *acceleration radius* [6] which specifies a lower bound on the isotropic acceleration of the end-effector from any admissible state. Another exception is the *motion isotropy hy-*

This work was supported through a NASA fellowship from Johnson Space Center under award No. NAG-9-1379. Any opinions, findings, and conclusions or recommendations expressed in this material are those of the authors and do not necessarily reflect the views of the National Aeronautics and Space Administration.

persurface [7] that generalizes the acceleration radius by handling the mismatch between translational and rotational coordinates, cf. [8]. The drawback of such analyses, however, is their emphasis on isotropic capabilities and worst-case performance. A manipulator may be highly efficient at accelerating its end-effector along some trajectories, even when its isotropic capabilities are diminished or lost altogether.

The goal of this paper is to provide further insight about the role that velocity plays for manipulability. Admittedly, this work raises more questions than answers. Although we advocate the use of general manipulability measures, the focus of this paper is more cautionary: Rather than propose a new measure of manipulability, we instead demonstrate that internal motion of a manipulator as well as movement of its end-effector can have a complex, non-negligible effect on a robot’s acceleration performance.

II. DYNAMIC MANIPULABILITY

Ignoring the effects of disturbances, e.g., friction, the equation of motion for an open-chain manipulator with n rigid links can be expressed as

$$\boldsymbol{\tau} = \mathbf{M}(\mathbf{q})\ddot{\mathbf{q}} + \mathbf{C}(\mathbf{q}, \dot{\mathbf{q}}) + \mathbf{G}(\mathbf{q}), \quad (1)$$

where $\boldsymbol{\tau}$ is an $n \times 1$ vector of joint actuator torques and \mathbf{q} , $\dot{\mathbf{q}}$, and $\ddot{\mathbf{q}}$ are $n \times 1$ vectors of generalized joint positions, velocities, and accelerations, respectively. In Eq. (1), $\mathbf{M}(\mathbf{q})$ is the $n \times n$ mass matrix that captures the configuration-dependent inertial properties of the robot, $\mathbf{C}(\mathbf{q}, \dot{\mathbf{q}})$ accounts for Coriolis and centrifugal forces, and $\mathbf{G}(\mathbf{q})$, represents the vector of joint torques due to gravity.

Let $\mathbf{x} = [x_1 \ x_2 \ \cdots \ x_m]^T$ denote the m -dimensional task vector associated with the tip of the manipulator. In the remainder of this paper we consider only translational accelerations and so \mathbf{x} is the Cartesian position of the end-effector with $m \leq 3$. The mapping of positions from joint space to task space is nonlinear, and the $m \times n$ Jacobian matrix \mathbf{J} represents the first-order term in a Taylor expansion of this mapping. Thus the Jacobian also describes the configuration-dependent relationship between velocities in the two coordinate systems:

$$\dot{\mathbf{x}} = \mathbf{J}(\mathbf{q})\dot{\mathbf{q}}. \quad (2)$$

Differentiating Eq. (2) with respect to time yields the corresponding relationship for accelerations:

$$\ddot{\mathbf{x}} = \mathbf{J}(\mathbf{q})\ddot{\mathbf{q}} + \dot{\mathbf{J}}(\mathbf{q}, \dot{\mathbf{q}})\dot{\mathbf{q}}. \quad (3)$$

A. Ellipsoid Derivation

Since the manipulator mass matrix is positive definite and, therefore, invertible, we can solve Eq. (1) for $\ddot{\mathbf{q}}$ and substitute into Eq. (3). Dropping the explicit dependencies on \mathbf{q} and $\dot{\mathbf{q}}$, the result is the following expression in terms of actuator torques rather than joint accelerations:

$$\ddot{\mathbf{x}} = \mathbf{J}\mathbf{M}^{-1}(\boldsymbol{\tau} - \mathbf{C} - \mathbf{G}) + \dot{\mathbf{J}}\dot{\mathbf{q}} \quad (4)$$

$$= \mathbf{J}\mathbf{M}^{-1}\boldsymbol{\tau} + \ddot{\mathbf{x}}_{vel} + \ddot{\mathbf{x}}_{grav}, \quad (5)$$

where

$$\ddot{\mathbf{x}}_{vel} = -\mathbf{J}\mathbf{M}^{-1}\mathbf{C} + \dot{\mathbf{J}}\dot{\mathbf{q}} \quad (6)$$

and

$$\ddot{\mathbf{x}}_{grav} = -\mathbf{J}\mathbf{M}^{-1}\mathbf{G}. \quad (7)$$

As in ref. [5], if we assume symmetric torque limits such that

$$-\tau_i^{limit} \leq \tau_i \leq +\tau_i^{limit}, \quad i = 1, \dots, n, \quad (8)$$

then the normalized actuator torques, $\tilde{\boldsymbol{\tau}}$, can be written as

$$\tilde{\boldsymbol{\tau}} = \mathbf{L}^{-1}\boldsymbol{\tau}, \quad (9)$$

where $\mathbf{L} = \text{diag}(\tau_1^{limit}, \dots, \tau_n^{limit})$. The set of admissible torques can then be represented as $2n$ inequalities written in the following compact form [5]:

$$\|\tilde{\boldsymbol{\tau}}\|_\infty \leq 1. \quad (10)$$

Substituting $\mathbf{L}\tilde{\boldsymbol{\tau}}$ for $\boldsymbol{\tau}$ in Eq. (5) yields

$$\ddot{\mathbf{x}} = \mathbf{J}\mathbf{M}^{-1}\mathbf{L}\tilde{\boldsymbol{\tau}} + \ddot{\mathbf{x}}_{vel} + \ddot{\mathbf{x}}_{grav} \quad (11)$$

$$= \mathbf{J}\mathbf{M}^{-1}\mathbf{L}\tilde{\boldsymbol{\tau}} + \ddot{\mathbf{x}}_{bias}, \quad (12)$$

where $\ddot{\mathbf{x}}_{bias} = \ddot{\mathbf{x}}_{vel} + \ddot{\mathbf{x}}_{grav}$ is a bias term that represents the end-effector acceleration when $\tilde{\boldsymbol{\tau}} = \mathbf{0}$.

Eq. (12) maps the n -dimensional hypercube defined by $\|\tilde{\boldsymbol{\tau}}\|_\infty \leq 1$ to an m -dimensional polytope that delimits the set of feasible end-effector accelerations. Alternatively, Eq. (12) can be used to map the n -dimensional sphere defined by

$$\tilde{\boldsymbol{\tau}}^T \tilde{\boldsymbol{\tau}} \leq 1 \quad (13)$$

to an m -dimensional ellipsoid. This *dynamic manipulability ellipsoid* is derived by solving Eq. (12) for $\tilde{\boldsymbol{\tau}}$ and substituting the result into Eq. (13):

$$(\ddot{\mathbf{x}} - \ddot{\mathbf{x}}_{bias})^T (\mathbf{J}\mathbf{M}^{-1}\mathbf{L})^{-T} (\mathbf{J}\mathbf{M}^{-1}\mathbf{L})^{-1} (\ddot{\mathbf{x}} - \ddot{\mathbf{x}}_{bias}) \leq 1. \quad (14)$$

Since \mathbf{M} and \mathbf{L} are both symmetric, Eq. (14) simplifies to

$$(\ddot{\mathbf{x}} - \ddot{\mathbf{x}}_{bias})^T (\mathbf{J}^{-T}\mathbf{M}\mathbf{L}^{-2}\mathbf{M}\mathbf{J}^{-1}) (\ddot{\mathbf{x}} - \ddot{\mathbf{x}}_{bias}) \leq 1. \quad (15)$$

The matrix $\mathbf{J}^{-T}\mathbf{M}\mathbf{L}^{-2}\mathbf{M}\mathbf{J}^{-1}$ from the previous equation determines the shape of the dynamic manipulability ellipsoid. Each eigenvector, \mathbf{v}_i , of this matrix specifies one of the ellipsoid's principal axes, the length of which is given by $1/\sqrt{w_i}$, where w_i is the corresponding eigenvalue. The shape of the "kinematic" manipulability ellipsoid, on the other hand, is determined by $\mathbf{J}^{-T}\mathbf{J}^{-1}$, with no correction for the manipulator's inertia and actuator torque limits.

To compute the actual ellipsoid, we require a suitable inverse for the Jacobian, which, in general, is not square. Following the recommendation by Chiacchio [5] we utilize the weighted pseudoinverse of the Jacobian:

$$\mathbf{J}_Q^\dagger = \mathbf{Q}^{-1}\mathbf{J}^T(\mathbf{J}\mathbf{Q}^{-1}\mathbf{J}^T)^{-1}, \quad (16)$$

where $\mathbf{Q} = \mathbf{M}\mathbf{L}^{-2}\mathbf{M}$ is a weight matrix that accounts for both inertia and torque limits. In summary, the shape of the "weighted" dynamic manipulability ellipsoid is determined by the eigenvectors and eigenvalues of

$$\mathbf{N} = \mathbf{J}_Q^{\dagger T} \mathbf{Q} \mathbf{J}_Q^\dagger. \quad (17)$$

See ref. [5] for further details.

B. Velocity Effects

Chiacchio *et al.* [4] demonstrated previously that $\ddot{\mathbf{x}}_{grav}$ has the effect of translating the center of the dynamic manipulability ellipsoid away from the origin where $\ddot{\mathbf{x}} = \mathbf{0}$. Even small translations can have a dramatic effect on the achievable accelerations in some directions, especially when $\ddot{\mathbf{x}}_{grav}$ is aligned approximately with the ellipsoid's minor axis. Eqs. (11)-(15) show that the velocity dependent terms from Eq. (6) have a similar effect on dynamic manipulability. Moreover, the overall displacement given by $\ddot{\mathbf{x}}_{bias}$ is sometimes dominated by $\ddot{\mathbf{x}}_{vel}$ as demonstrated in the following section.

Returning for the moment to Eq. (1), one can show that $\mathbf{C}(\mathbf{q}, \dot{\mathbf{q}})$ is bounded by a quadratic in $\dot{\mathbf{q}}$ such that

$$\|\mathbf{C}(\mathbf{q}, \dot{\mathbf{q}})\| \leq c(\mathbf{q})\|\dot{\mathbf{q}}\|^2, \quad (18)$$

where $c(\mathbf{q})$ is a known scalar function specified by the manipulator's inertial properties and $\|\cdot\|$ is any appropriate norm [9]. Moreover, if the joints are all revolute, then $c(\mathbf{q})$ becomes a constant independent of configuration [9]. And since \mathbf{M}^{-1} is bounded [10], one can derive similar relationships for both terms in Eq. (6) and, therefore, for $\ddot{\mathbf{x}}_{vel}$ as well:

$$\|\ddot{\mathbf{x}}_{vel}(\mathbf{q}, \dot{\mathbf{q}})\| \leq \beta(\mathbf{q})\|\dot{\mathbf{q}}\|^2, \quad (19)$$

where $\beta(\mathbf{q})$ is another known scalar function of \mathbf{q} .

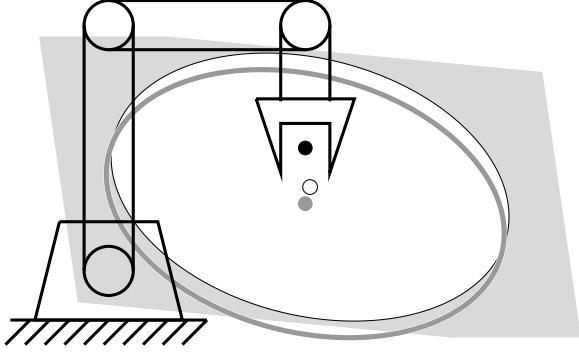


Fig. 1. Acceleration polytope and dynamic manipulability ellipsoids for $\mathbf{q} = [+ \frac{\pi}{2} \ - \frac{\pi}{2} \ - \frac{\pi}{2}]^T$ and $\dot{\mathbf{q}} = [1 \ 1 \ 1]^T$. The polytope (light gray) and corresponding ellipsoid (white cutout) depict the manipulator's acceleration capabilities with corrections for both gravity and velocity. Superimposed is the dynamic manipulability ellipsoid with correction for gravity only (dark gray). Small circles denote the position of the end-effector (black), the centroid of the polytope (white), and the center of the gravity-corrected ellipsoid (gray).

Eq. (19) provides further intuition about the effects of velocity on manipulability. Nominally, we expect the acceleration bias to be quadratic in the joint velocity. However, Eq. (19) represents an upper bound and provides no indication for which configurations $\|\ddot{\mathbf{x}}_{vel}\|$ is small even when $\|\dot{\mathbf{q}}\|^2$ is relatively large. Eq. (19) also fails to capture the orientation of $\ddot{\mathbf{x}}_{vel}$ which can change dramatically over a short period of time. Theoretical limitations such as these motivate the use of case studies to gain further insight about the role that velocity plays for manipulability.

III. EXAMPLES

The examples studied in this section all utilize the planar three-link manipulator described by Chiacchio [5]. Each link is modeled as a rigid rod with uniform density and with inertial parameters set as follows:

link	length (m)	mass (kg)
1	1.0	4.0
2	0.8	2.0
3	0.5	0.6

Eq. (1) summarizes the manipulator dynamics, with gravity acting downward and with actuator torques normalized by $\mathbf{L} = \text{diag}(100, 30, 4)$ Nm.

A. Increasing Velocity

Our first case study replicates one by Chiacchio [5] with the addition of a velocity component. In particular, we examine the configuration $\mathbf{q} = [+ \frac{\pi}{2} \ - \frac{\pi}{2} \ - \frac{\pi}{2}]^T$ with joint velocities $\dot{q}_1 = \dot{q}_2 = \dot{q}_3 = \omega$, for ω increasing from 0 to 4 $\text{rad} \cdot \text{s}^{-1}$. For the case $\omega = 1$ we have

$$\mathbf{M} = \begin{bmatrix} 4.494 & 0.711 & -0.100 \\ 0.711 & 0.861 & 0.050 \\ -0.100 & 0.050 & 0.050 \end{bmatrix},$$

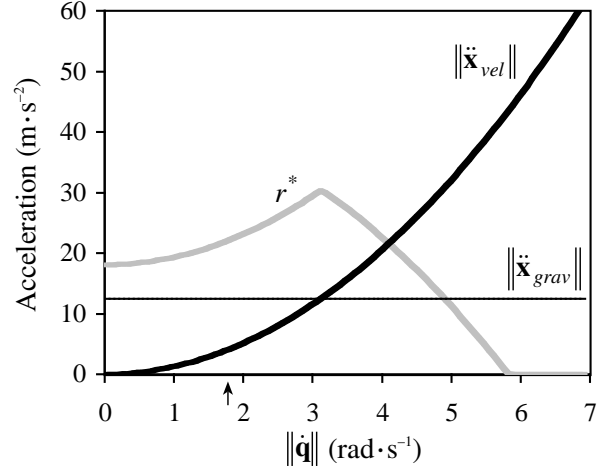


Fig. 2. Acceleration versus joint velocity magnitude with $\dot{q}_1 = \dot{q}_2 = \dot{q}_3 = \omega$. Shown are the acceleration radius (gray curve) and the magnitude of the acceleration offsets due to gravity and velocity (light and heavy curves, respectively). The small arrow marks the value of $\|\dot{\mathbf{q}}\|$ that corresponds to $\omega = 1$ as in Figure 1.

$$\mathbf{C} = [4.440 \quad -0.680 \quad -0.480]^T,$$

$$\mathbf{G} = [12.569 \quad 12.570 \quad 0.000]^T,$$

$$\mathbf{J} = \begin{bmatrix} -0.500 & 0.500 & 0.500 \\ 0.800 & 0.800 & 0.000 \end{bmatrix},$$

and

$$\mathbf{J}\dot{\mathbf{q}} = [-3.200 \quad 3.500]^T.$$

From Eqs. (6) and (7) we then derive

$$\ddot{\mathbf{x}}_{vel} = [1.072 \quad 3.697]^T$$

and

$$\ddot{\mathbf{x}}_{grav} = [0.000 \quad -12.400]^T.$$

Thus for $\omega = 1$, $\|\ddot{\mathbf{x}}_{grav}\|$ is more than three times greater than $\|\ddot{\mathbf{x}}_{vel}\|$. In this case, the overall translation given by $\ddot{\mathbf{x}}_{bias}$ is attributed primarily to the gravity component, as exhibited by a small offset between the ellipsoids in Figure 1.

Nevertheless, Figure 2 shows that $\ddot{\mathbf{x}}_{vel}$ grows quadratically in $\|\dot{\mathbf{q}}\|$ as expected. (Empirically, Eq. (19) holds with equality for $\beta = 1.28$.) In this particular example, the inner product of $\ddot{\mathbf{x}}_{vel}$ and $\ddot{\mathbf{x}}_{grav}$ is negative, and so $\ddot{\mathbf{x}}_{vel}$ cancels part of the offset due to gravity. For $\|\dot{\mathbf{q}}\| < 3$, the effect is improved isotropic capabilities, as indicated by the increased acceleration radius, r^* . When velocity grows beyond $\|\dot{\mathbf{q}}\| = 3$, however, r^* decreases toward zero, since $\ddot{\mathbf{x}}_{vel}$ grows large enough to dominate $\ddot{\mathbf{x}}_{grav}$ and eventually the polytope no longer encompasses the end-effector.¹

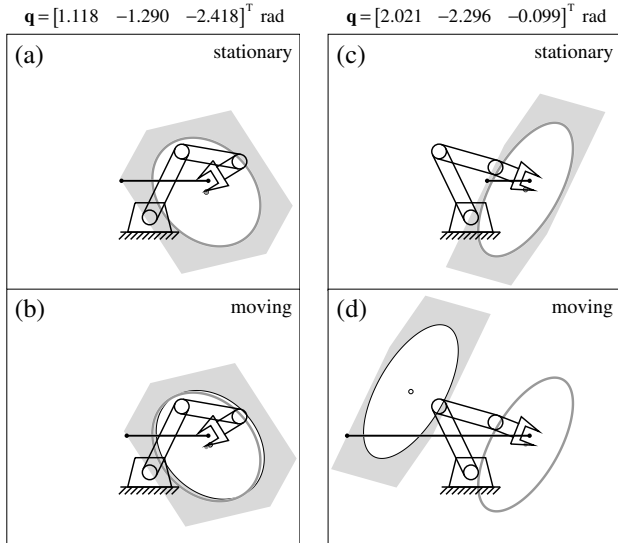


Fig. 3. Acceleration polytope and dynamic manipulability ellipsoids for two configurations that maintain the end-effector position at $(0.8, 0.5)$. Maximum achievable acceleration in the leftward direction is depicted by a horizontal line from the end-effector to the leftmost point on the polytope. When the manipulator is stationary, the configuration in panel (a) is preferred to that in panel (c). This contrasts with a moving robot, for which the configuration in panel (d) is preferred to the one in panel (b).

B. Exploiting Redundancy

It is well known that redundancy can complicate a control problem but, at the same time, can expand the capabilities of a robot, e.g., for singularity avoidance. One approach for dealing with redundancy is to use heuristic strategies derived from theoretical considerations. For instance, Chiacchio [11] suggested that for minimum-time control, one could exploit redundancy to align more closely the surface of the acceleration ellipsoid with the tangent to the task space path. In this section we demonstrate that redundancy can also be used to reconfigure a robot such that internal motion improves the acceleration capabilities along some prespecified direction.

Consider the manipulator shown previously in Figure 1, and suppose we wish to reconfigure this robot to maximize the achievable leftward acceleration of the end-effector. In this scenario we also require that the end-effector position remain constant until the reconfiguration is (nearly) complete. One possible solution is to search for the best static posture, with the gravity-corrected acceleration polytope as a means for evaluation. Figure 3a shows the outcome of this search, and the small offset between ellipsoids in Figure 3b illustrates that velocity (for movement as described shortly) has little effect at the resulting configuration.

¹As defined in [6], the acceleration radius represents the size of the largest sphere which is centered on the end-effector and fits within every acceleration polytope over the entire operating range of the manipulator. In this paper, we relax the latter requirement and plot r^* separately for each state.

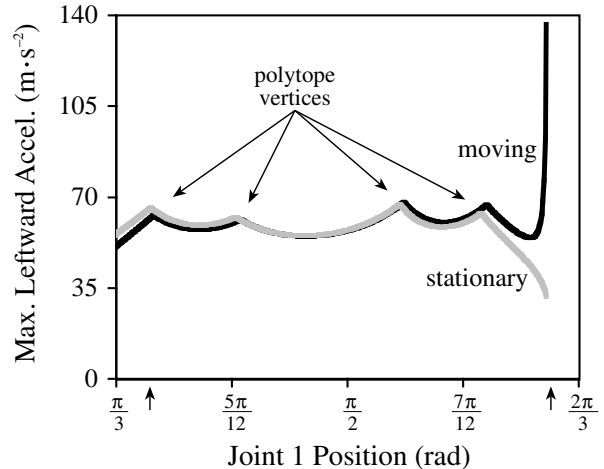


Fig. 4. Maximum leftward acceleration achievable at each position of joint 1. Shown are two conditions where the manipulator is stationary (gray curve) or moving (black curve). Local extrema occur whenever the active torque constraint changes at a polytope vertex. Small arrows mark the values of q_1 that correspond to the configurations shown Figure 3.

However, if we repeat the search while evaluating the polytope corrected for velocity as well as gravity, then the outcome is an entirely different posture with more than twofold improvement in leftward acceleration. Shown in Figure 3d, this result was generated for the case where joint 1 moves at a constant speed of $1 \text{ rad} \cdot \text{s}^{-1}$ and the remaining joints move in accordance with the inverse kinematics solution given q_1 . As summarized in Figure 4, $\ddot{\mathbf{x}}_{vel}$ makes little difference in the maximum leftward acceleration until the manipulator approaches the configuration $\mathbf{q} = [2.02 \quad -2.34 \quad 0.00]^T$, where the two distal-most links become aligned.

C. Raising A Payload

Our final case study demonstrates the benefits of passing through a singularity when raising a heavy payload. From the previous example we saw that when two links become nearly aligned, motion can lead to large displacements of the acceleration polytope and, therefore, to large discrepancies between analyses that assume the robot is either stationary or not. Large displacements of the polytope can be critical, perhaps catastrophic, to the task at hand. Nevertheless, the example in Figure 3d illustrates the potential benefits of large values for $\ddot{\mathbf{x}}_{vel}$. However, this example is unrealistic because we assumed that Cartesian position remains fixed, even when the polytope is displaced enough that translation of the end-effector is unavoidable. In this section we make no such assumptions and, instead, perform *a posteriori* analysis of the trajectory that emerges from a dynamic simulation of the robot.

Figure 5 illustrates one such trajectory with a 6.5 kg payload. The robot's task is to raise the payload from the straight-down, stable equilibrium to the straight-up, unsta-

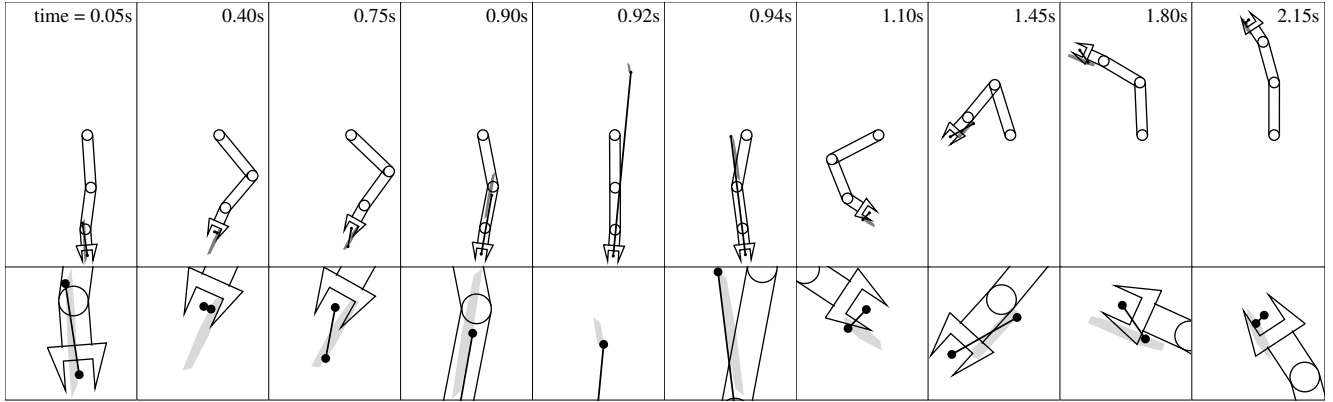


Fig. 5. Raising a 6.5 kg payload to the unstable equilibrium. The acceleration attained at each time step is depicted as a vector from the end-effector to a point within the acceleration polytope (gray). Close-ups of the polytope are shown in the lower panels.

ble equilibrium. Limited torque restricts the class of feasible solutions to those that execute a coordinated swing, i.e., those that exploit momentum and intersegmental dynamics. The robot achieved this coordination by switching between two sets of proportional-derivative feedback controllers—with the reference points and feedback gains, as well as the switch time, set by a trial-and-error learning algorithm [12].

Perhaps the most prominent feature of Figure 5 is the relatively small size of the acceleration polytope. (Close-ups are shown in the lower panels of the figure.) As expected, the heavy payload has an adverse effect on those capabilities attributed to the size and shape of the polytope. However, the payload does not necessarily impair the robot’s ability to generate a wide range of accelerations at the required moments. This is evidenced by the varied orientation and magnitude of the vectors depicted in Figure 5.

Of particular interest from this example is motion leading to the singularity near time $t = 0.92$ s (frame five of Figure 5). At $t = 0.05$ s all three joint actuators operate at their torque limits and the corresponding end-effector acceleration lies at a vertex of the polytope. Close to time $t = 0.40$ s the robot, with low velocity, achieves a posture that facilitates the next phase of the movement. In particular, at $t = 0.75$ s the manipulator begins a downward acceleration toward the singularity, and by $t = 0.92$ s, a large vertical acceleration “kicks” the payload upward.

As suggested by Figure 6a, the upward kick is due almost entirely to the large value of $\ddot{\mathbf{x}}_{vel}$ induced by motion near the singularity. The singularity appears to offer an efficient means for “focusing” kinetic energy to produce movement in a particular direction. With a shorter effective moment arm against gravity, the manipulator then appears well suited to generate potential energy. After about $t = 1.5$ s, the remainder of the movement deals primarily with the coordinated transfer of kinetic energy to potential energy, rather than the production of additional energy for the system. (See Figure 6b.)

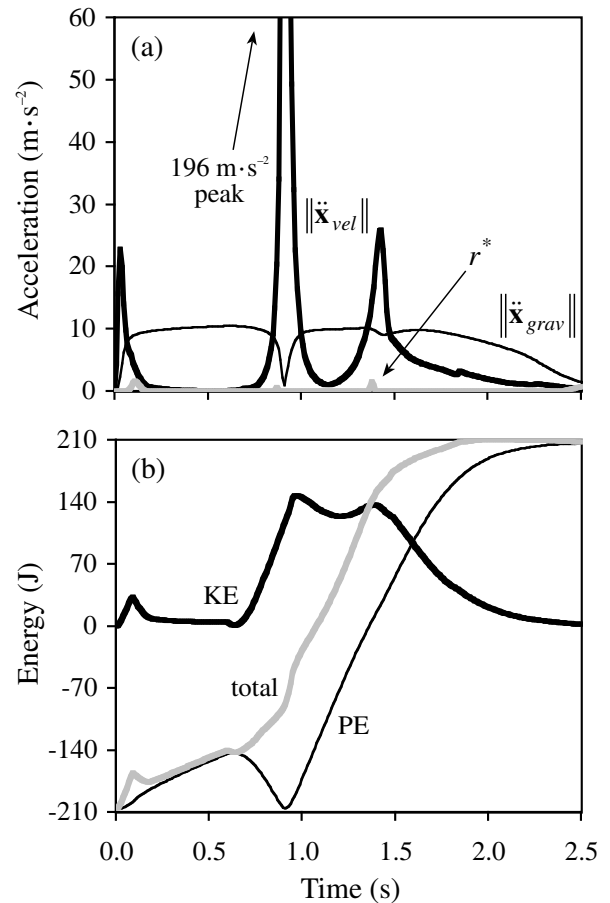


Fig. 6. Acceleration (a) and energy (b) versus time for the trajectory illustrated in Figure 5. Shown in the upper plot (a) are the acceleration radius (gray curve, barely visible) and the magnitude of the acceleration offsets due to gravity and velocity (light and heavy curves, respectively). Shown in the lower plot (b) are potential, kinetic, and total energy during the movement (light, heavy, and gray curves, respectively).

IV. SUMMARY AND CONCLUSIONS

Measures of manipulability are often intended as a description of a robot’s capabilities—before specification of

a task. Implicit in such measures is the assumption that the robot is either motionless (cf. dynamic manipulability measure [1]) or moving slowly (cf. acceleration radius [6]). Although we agree that analysis of stationary manipulators is “fundamental” [1] for a deeper understanding of the relationship between manipulability ellipsoids and performance, in this paper we demonstrated that motion has a complex, non-negligible effect on dynamic manipulability.

With the example in Figure 5, for instance, we saw that motion-dependent displacement of the acceleration polytope plays a more instrumental role than the polytope size or shape. This example was a somewhat extreme demonstration that, with some tasks, it may be desirable for the robot’s capabilities to be momentarily skewed one way or another. The relationship between control signal and ellipsoid (or polytope) is complex as well. Though not obvious from Figure 5, some actuator commands appear to drive the robot toward a desired posture, whereas others seem to reposition the polytope in anticipation of future needs. We interpret these subtle complexities, not as an inability on the part of the robot, but rather as an impediment for the design of a suitable control system. For this reason (and others) we believe that intelligent control and machine learning techniques will become more prevalent for manipulator control.

We also demonstrated that the acceleration polytope is helpful for *a posteriori* analysis of an emergent trajectory. The challenge is to incorporate velocity-dependent effects as part of *a priori* analysis of manipulability. Can one still use the acceleration polytope (or ellipsoid) to determine favorable postures with which to bias a trajectory planner or learning algorithm? Our results suggest that this goal is a difficult undertaking, especially for manipulators that move at high speed. However, the example in Section III-C provides evidence that singular configurations may be useful in this regard.

Wang *et al.* [13] also observed the benefits of singular configurations. Their work extended the payload capacity of a Puma industrial robot by formulating an optimal control problem and by solving the corresponding nonlinear optimization problem. Singular configurations were explicitly part of neither the problem nor the solution technique, yet the best trajectories routinely passed through singularities. Wang *et al.* offered the following explanation [13]: Singular configurations are beneficial because the robot structure supports heavy loads, thereby freeing the actuators to contribute increased torque for some other aspect of the task.

This interpretation is consistent with “kinematic” manipulability based on the Jacobian alone, i.e., the enhanced static force transmission near singularities. Our results, however, suggest that dynamic effects are important as well. In particular, we demonstrated that large displacements of the acceleration polytope occur for motion near

singular configurations. These results, like other measures of *dynamic* manipulability, describe the capabilities of the robot and its actuators, whereas the static force ellipsoid describes the mapping between end-effector force and net joint torque—with no explicit role for the actuators.

Finally, as summarized by Eq. (19), displacement of the acceleration polytope is bounded by a quadratic in the joint velocity. This theoretical result could serve as the basis for setting a velocity threshold, below which velocity effects can be safely ignored. Nevertheless, the existence of a more useful characterization of velocity-dependent dynamic manipulability remains an open question. The desideratum, then, is an analogue of the manipulability ellipsoid—one that describes the way arbitrary joint-space velocities are mapped to displacements of the acceleration polytope.

REFERENCES

- [1] Tsuneo Yoshikawa, “Manipulability of robot mechanisms,” *The International Journal of Robotics Research*, vol. 4, no. 2, pp. 3–9, 1985.
- [2] Stephen L. Chiu, “Task compatibility of manipulator postures,” *The International Journal of Robotics Research*, vol. 7, no. 5, pp. 13–21, 1988.
- [3] Tsuneo Yoshikawa, “Dynamic manipulability of robot manipulators,” *Journal of Robotic Systems*, vol. 2, no. 1, pp. 113–124, 1985.
- [4] P. Chiacchio, S. Chiaverini, L. Sciavicco, and B. Siciliano, “Influence of gravity on the manipulability ellipsoid for robot arms,” *Journal of Dynamic Systems, Measurement, and Control*, vol. 114, no. 4, pp. 723–727, 1992.
- [5] Pasquale Chiacchio, “A new dynamic manipulability ellipsoid for redundant manipulators,” *Robotica*, vol. 18, no. 4, pp. 381–387, 2000.
- [6] Timothy J. Graettinger and Bruce H. Krogh, “The acceleration radius: a global performance measure for robotic manipulators,” *IEEE Journal of Robotics and Automation*, vol. 4, no. 1, pp. 60–69, 1988.
- [7] Alan Bowling and Oussama Khatib, “The motion isotropy hypersurface: a characterization of acceleration capability,” in *Proceedings of the IEEE/RSJ International Conference on Intelligent Robots and Systems*, 1998, vol. 2, pp. 965–971.
- [8] Keith L. Doty, Claudio Melchiorri, Eric M. Schwartz, and Claudio Bonivento, “Robot manipulability,” *IEEE Transactions on Robotics and Automation*, vol. 11, no. 3, pp. 462–468, 1995.
- [9] F. L. Lewis, C. T. Abdallah, and D. M. Dawson, *Control of Robot Manipulators*, Macmillan Publishing Company, New York, 1993.
- [10] John J. Craig, *Adaptive Control of Mechanical Manipulators*, Addison-Wesley Publishing Company, Reading, MA, 1988.
- [11] Pasquale Chiacchio, “Exploiting redundancy in minimum-time path following robot control,” in *Proceedings of the 1990 American Control Conference*, 1990, vol. 3, pp. 2313–2318.
- [12] Michael T. Rosenstein and Andrew G. Barto, “Robot weightlifting by direct policy search,” in *Proceedings of the Seventeenth International Joint Conference on Artificial Intelligence*, Bernhard Nebel, Ed., San Francisco, 2001, vol. 2, pp. 839–844, Morgan Kaufmann.
- [13] Chia-Yu E. Wang, Wojciech K. Timoszyk, and James E. Bobrow, “Payload maximization for open chained manipulators: finding weightlifting motions for a Puma 762 robot,” *IEEE Transactions on Robotics and Automation*, vol. 17, no. 2, pp. 218–224, 2001.